Colocalization of Quantum Dots by Reactive Molecules Carried by Motor Proteins on Polarized Microtubule Arrays

Kazuya Fujimoto,[†] Masuto Kitamura,[†] Masatoshi Yokokawa,[†] Isaku Kanno,[†] Hidetoshi Kotera,[†] and Ryuji Yokokawa*[,†,‡]

[†]Department of Micro Engineering, Kyoto University, Yoshida-Honmachi, Sakyo, Kyoto 606-8501, Japan and [‡]Precursory Research for Embryonic Science and Technology (PRESTO), Japan Science and Technology Agency (JST), 4-1-8 Honcho, Kawaguchi, Saitama 332-0012, Japan

ABSTRACT The field of microfluidics has drastically contributed to downscale the size of benchtop experiments to the dimensions of a chip without compromising results. However, further miniaturization and the ability to directly manipulate individual molecules require a platform that permits organized molecular transport. The motor proteins and microtubules that carry out orderly intracellular transport are ideal for driving *in vitro* nanotransport. Here, we demonstrate that a reconstruction of the cellular kinesin/dynein–microtubule system in nanotracks provides a molecular total analysis system (MTAS) to control massively parallel chemical reactions. The mobility of kinesin and a microtubule dissociation method enable orientation of a microtubule in an array for directed transport of reactive molecules carried by kinesin or dynein. The binding of glutathione S-transferase (GST) to glutathione (GSH) and the binding of streptavidin to biotin are visualized as colocalizations of quantum dots (Q-dots) when motor motilities bring them into contact. The organized nanotransport demonstrated here suggests the feasibility of using our platform to perform parallel biochemical reactions focused at the molecular level.

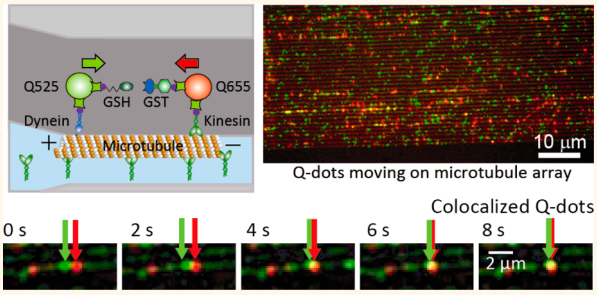

KEYWORDS: μTAS · motor proteins · molecular transport · kinesin · dynein · nanostructures

Since the concept of miniaturized chemical analysis systems was introduced by Manz *et al.*,[1] numerous on-chip technologies have been demonstrated to realize biochemical reactions, analyses, and detections including protein and DNA separations,[2–4] PCR,[5,6] and immunoassays in proteomics.[7] Some of these technologies have been integrated to micro total analysis systems (μTAS), and already commercialized for practical uses.[8,9] Enhancing the throughput of μTAS toward further massive and parallel assay in such as high-throughput drug screening is a next challenge in the field. Although multiplexing microfluidic components or optimizing assay sequences for a specific target are dominant approaches, downsizing μTAS by focusing on a countable number of molecules is another promising direction. Besides manipulating a small amount of liquid solution containing target molecules within nanofluidic channels,[10] researchers explored a method to directly manipulate the molecules by motor proteins in μTAS. For the past decade, motor protein–driven nanotransport using gliding assay–based systems (molecular shuttles) has been used to transport cargos,[11–13] load and unload cargos,[14,15] and control bioassays.[12,16,17] The motor proteins have been designed to utilize motor functions to manipulate cargo molecules as done by liquid solution in μTAS. However, the reported systems lack the ability to regulate the direction of molecular transport without external biases or structures owing to the use of only plus end-directed kinesin motors.[18–21] Scale-down is also limited to a lab-on-a-chip scale, because assays are performed by perfusing solutions containing target molecules, requiring that numerous molecules are transported on microtubules.[12,22] Manipulating

* Address correspondence to ryuji@me.kyoto-u.ac.jp.

Received for review September 28, 2012 and accepted December 11, 2012.

Published online December 11, 2012
10.1021/nn3045038

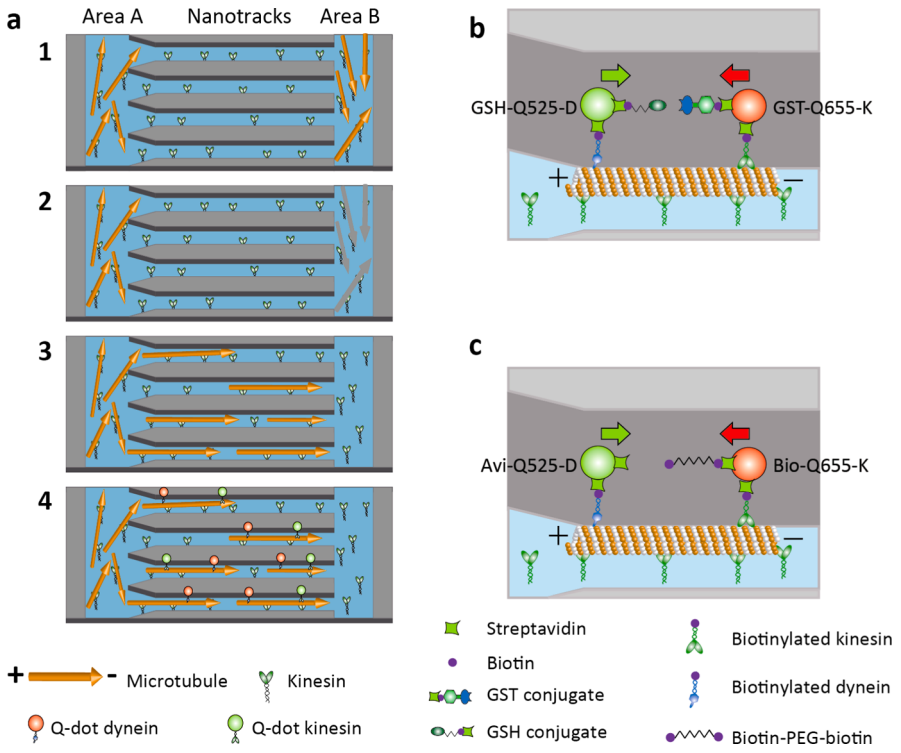

Figure 1. Conceptual basis of the molecular total analysis system (MTAS). (a) Assay sequence to orient microtubule polarity and Q-dot assay. (b) Representation of the mode of binding of GST to GSH. (c) Representation of the mode of binding of streptavidin to biotin.

fewer molecules is necessary to minimize the system and increase the throughput of chemical reactions.

In contrast to these limitations, intracellular transport shows well-organized bidirectional nanotransport of individual molecules or vesicles, which is supported by microtubules preorganized for cargo transport by kinesin and dynein.[23,24] It can be reconstructed *in vitro* as a bead assay-based system by fixing microtubules on a glass substrate and allowing motors to carry cargos toward the direction defined by the polarities of the microtubules.[25−27] Application-oriented assay reported by Carroll-Portillo *et al.* demonstrated the Q-dot transport following a sandwich assay targeting TNF-α.[28] In this assay, however, transport direction relied on randomly immobilized microtubules, and the sandwich assays were achieved by passively diffusing TNF-α and anti-TNF-α-labeled Q-dot. Although several technical solutions have been presented including polarity orientation of microtubules and Q-dot assays, intracellular transport is not yet applicable to practical applications. Two important technical challenges to realize further organized molecular systems based on a bead assay-based system are controlling the cargo transport direction by defining the polarities of individual microtubules and employing both kinesin and dynein to actively and bidirectionally transport cargos for biochemical assays. Therefore, our approach here is to tackle these two challenges: One is to define polarities of individual microtubules to form a microtubule array in a massive and parallel manner. The other is to actively induce chemical reactions of reactive molecules transported by kinesin and dynein motors. This enables miniaturization of μTAS to a molecular total analysis system (MTAS), where microfluidic channels and chemical reactions in μTAS correspond to microtubules (roads to carry target molecules) and Q-dot colocalizations (individual molecular reactions) in MTAS, respectively.

The bead assay-based system using multiple motors was reconstructed in a nanotrack array that regulates the direction of molecular transport and the physical interaction of target molecules (Figure 1a). Two areas at the end of the array, named A and B (400 μm × 1000 μm each), were prepared on a coverslip by patterning aluminum and an electron beam resist (see Materials and Methods for details). To guide microtubules into the nanotracks, one end was widened to form a V-shape with an 8.5° angle, and aluminum was overetched to provide a submicrometer-sized overhang structure (Figure 2a). A flow cell was constructed and treated with Pluronic, resulting in a coating of only the glass surface with kinesin (this assay protocol is in Supporting Information section 1).[29−32] Microtubules were injected perpendicular to the nanotrack array so that they adhered mostly to areas A and B (Figure 1a-1) and could glide spontaneously into nanotracks from both areas. The V-shape structures increased a ratio of microtubules gliding from area A to B. Moreover, as discussed below, we also dissociated the microtubules to further increase the ratio by eliminating microtubules in area B, which is shown as gray arrows in Figure 1a-2. After

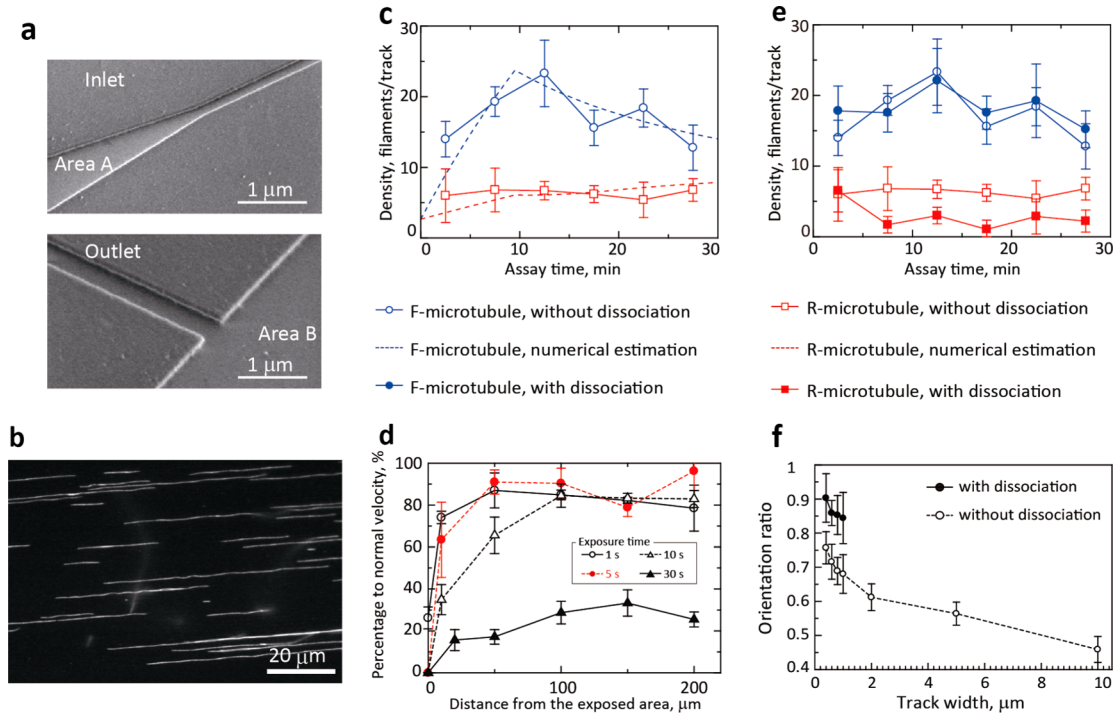

Figure 2. Optimization and evaluation of the microtubule array. (a) Nanotrack inlet and outlet patterned on a glass substrate. (b) Microtubule array with defined polarities. (c) Microtubule density per 400-nm-wide nanotrack (mean ± SE, *N* = 10 nanotracks). Blue open circles and red open squares indicate F-microtubules and R-microtubules, respectively. Data from numerical estimations are plotted as broken lines. (d) Gliding velocity of microtubules (mean ± SE, *N* = 20) depending on the distance from the area exposed to light to initiate microtubule dissociation. (e) Microtubule density per 400-nm-wide nanotrack with or without microtubule dissociation (mean ± SE, *N* = 10). (f) Orientation ratio (mean ± SE) of microtubule polarity with or without microtubule dissociation.

immobilization of polarity-oriented microtubules by glutaraldehyde (Figure 1a-3, Figure 2b), we evaluated the motilities of kinesin- and dynein-conjugated Q-dots. As expected, kinesin-labeled Q-dots moved to the plus ends of microtubules, and dynein-labeled Q-dots moved in the other direction (Figure 1a-4). This reconstructed kinesin- and dynein-containing microtubule system permits massive and parallel nanotransport to move target molecules in designated directions *in vitro*.

Using this scheme, we demonstrated molecule-specific binding of GST to GSH and of streptavidin to biotin to evaluate the feasibility of the molecular system (Figure 1b,c). We bound GST and GSH to Q-dot 655 and Q-dot 525, respectively, by taking advantage of the strong interaction between streptavidin and biotin, resulting in GST−Q-dot 655−kinesin (GST-Q655-K) and GSH−Q-dot 525−dynein (GSH-Q525-D) (Figure 1b). Molecular transport resulting from the movements of kinesin and dynein caused a collision of the GST and GSH sequences, which was revealed by Q-dot colocalization. The binding of streptavidin to biotin was demonstrated using biotin-PEG-biotin−Q-dot 655−kinesin (bio-Q655-K) and streptavidin−Q-dot 525−dynein (avi-Q525-D) (PEG, polyethylene glycol; Figure 1c).

RESULTS AND DISCUSSION

Polar Orientation of Microtubule Arrays. Figure 2 summarizes experimental results obtained during the construction of the microtubule array. Analysis of changes in the density of microtubules in the 400 nm-wide nanotrack (Figure 2a) indicated that the V-shape structure increased the number of forward-moving microtubules (F-microtubules). However, the number of F-microtubules started to decrease after 10 min owing to a shortage of microtubules in area A. On the contrary, the density of microtubules gliding in the reverse direction (R-microtubules) was almost constant owing to a narrow outlet opening onto area B, which restricted movement regardless of the density in area B. Nanotrack width could be optimized within the range from 400 nm to 10 μm to evaluate the structural effect for aligning single microtubule filaments. Tracks wider than 2 μm showed smaller differences in the number of F-microtubules and R-microtubules than those on narrower tracks less than 1 μm (Supporting Information, Figure S1). This necessitated the development of rectifiers.[18] However, the structural effect was evident at widths less than 1 μm: whereas the densities of F-microtubules were similar among 400−1000 nm-wide tracks, mean densities of R-microtubules during 30-min assay decreased with reduced channel width (Supporting Information, Figure S2): 9.61 ± 0.65 filaments per track (mean ± SE, *N* = 31), 9.43 ± 0.58 filaments per track (*N* = 30), 8.10 ± 0.60 filaments per track (*N* = 31), 6.47 ± 0.48 filaments per track (*N* = 30) for 1 μm, 800 nm, 600 nm, and 400 nm-wide tracks, respectively. According

to the statistical significance of the decrease ($p < 0.01$; Student's t test), 400 nm-wide track is the most effective to suppress F-microtubules. The number of F-microtubules was maximal 10−15 min after starting the assay. The subsequent decrease could be explained by the gliding of microtubules through nanotracks (each 200 μm long) at a mean velocity of 0.34 ± 0.01 μm s^{-1} (mean ± SE, N = 20). Owing to the limited number of microtubules in area A and B, gliding of microtubules toward area B caused an irreversible decrease in F-microtubule density. The orientation ratio at the assay time of 10 min defined by dividing the number of F-microtubules by the total number of microtubules is shown in Figure 2f. Tracks wider than 5 μm, which have been used in the past,[18,33−36] yielded equal levels of F-microtubules and R-microtubules (ratio ≈ 0.5) because microtubules can make U-turns and glide randomly. Below the track width of 1 μm, it is experimentally and theoretically demonstrated that U-turns are effectively suppressed.[37] In addition to preventing U-turns, we could effect a significant difference in the number of F-microtubules and R-microtubules by the V-shape structure of narrow tracks less than 1 μm, which yielded a maximal orientation ratio of 0.76 ± 0.05 (mean ± SE).

This experimental result was supported by numerical analysis, with the assumption that (i) the number of gliding microtubules is proportional to density, (ii) there are no U-turns in nanotracks, (iii) no microtubules are found in the bulk solution, and (iv) channel width defines the probability of microtubule gliding into nanotracks. The number of microtubules on a nanotrack was estimated by calculating the microtubule density on a glass surface. Time-dependent microtubule density in area A, dD_A/dt, is expressed as the difference between the number of microtubules gliding in a nanotrack relative to those gliding out of a nanotrack, as shown in eq 1. $P_{out}D_{B(t - T_{th})}$ is the number of microtubules gliding out from a nanotrack to area A at time t, where P_{out} is the probability of microtubule introduction to a nanotrack per minute from area B, $D_{B(t)}$ is the density in area B, and T_{th} is time for microtubule passing through a nanotrack. The number of microtubules gliding into a nanotrack from area A at time t, $P_{in}D_{A(t)}$, is expressed in the same manner. The difference of these products is divided by the area A, A_{in}, to provide dD_A/dt. The corresponding equation can be derived for time-dependent microtubule density in area B, dD_B/dt, as shown in eq 2.

$$\frac{dD_A}{dt} = \frac{P_{out}D_{B(t - T_{th})} - P_{in}D_{A(t)}}{A_{in}} \quad (1)$$

$$\frac{dD_B}{dt} = \frac{P_{in}D_{A(t - T_{th})} - P_{out}D_{B(t)}}{A_{out}} \quad (2)$$

Then, as shown in eq 3, the number of microtubules moving in the forward direction per nanotrack at time t, $N_{f(t)}$, is expressed by integrating the product of probability and density during the period t to T_{th}. The corresponding number of microtubules gliding in the reverse direction, $N_{r(t)}$, is calculated by eq 4.

$$N_{f(t)} = \int_{t - T_{th}}^{t} P_{in}D_{A(t)}\, dt \quad (3)$$

$$N_{r(t)} = \int_{t - T_{th}}^{t} P_{out}D_{B(t)}\, dt \quad (4)$$

Variables and their initial values are summarized in Supporting Information, Table S1. Using these conditions, $N_{f(t)}$ and $N_{r(t)}$ are calculated with MATLAB software (MathWorks) for each assay period and plotted along with experimental results in Figure 2c and Supporting Information, Figure S2 as broken lines. The close agreement of the numerical analysis with experimental data revealed that we could not further reduce the number of R-microtubules by the structural effect only (Figure 2c).

To achieve a higher orientation ratio, it was essential to eliminate the R-microtubules from area B. To do this, we developed a microtubule dissociation method, which involves microtubule depolymerization following exposure to light (530−550 nm) in an oxygen-scavenging solution optimized referring components in the widely used oxygen-scavinging system,[38] while maintaining the activity of kinesin (see Supporting Information section 2 for details). This method employs oxygen radicals that dissociate microtubules in the designated area only. However, diffusion of oxygen radicals deteriorates microtubule gliding near the exposed area with prolonged exposure (Figure 2d). To minimize degradation of microtubule motility in the unexposed area while ensuring dissociation in the exposed area, we selected an exposure time of 5 s for microtubule orientation. Under this condition, the mean velocity recovered to 91.0 ± 11.4% (mean ± SD) of normal velocity at a distance 50 μm away from the exposed area.

The orientation of polarity was improved by using the microtubule dissociation method to greatly decrease the number of R-microtubules (Figure 2e, Figure S3). For 400-nm-wide nanotrack, the mean density of R-microtubules was decreased from 6.47 ± 0.48 filaments per track (mean ± SE, N = 30) to 2.23 ± 0.38 filaments per track (N = 35), resulting in the significant difference ($p < 0.01$; Student's t test). Compared to this decrease in the number of R-microtubules, the number of F-microtubules was retained, the trend being similar to that seen in an assay without the dissociation method (Figure 2c, Supporting Information, Figure S2). This results in the drastic change in orientation ratio, which is plotted in Figure 2f for widths less than 1 μm. It revealed that the orientation ratio increased with the decrease of track width and the highest orientation ratio (0.91 ± 0.04, mean ± SE) was produced with a track width of 400 nm (Supporting Information, Movie 1). Several groups including ours reported quantitative analysis of directional gliding of microtubules: bidirectional

gliding (presumably orientation ratio of 0.5 due to no control in gliding direction) on a nanoimprinted polymer surface was demonstrated,[31] over 70% of microtubules were rectified by arrowhead structures,[18] a similar approach reached ~93%,[34] and over 95% of kinesin-coated beads were unidirectionally transported on microtubules oriented by fluid shear stress.[19] However, none of the previously reported results indicate polarity orientation of individual microtubules in the designated unidirectional direction at a specific location on a chip, which is significant in MTAS to realize the directional cargo transport. In this engineering point of view, we first demonstrated that almost all microtubules are gliding unidirectionally and individually on parallel nanotracks, even the ratio of 0.91 is not highest among reported results. For subsequent experiments, according to the statistical analysis showing the significant decrease of R-microtubules on narrower tracks and to avoid overlap of multiple microtubules on a track, we selected a track width of 400 nm with 1 μm spacing as an optimum structure to orient single microtubule filaments with the microtubule dissociation method. After microtubule immobilization by glutaraldehyde (Figure 2b), we monitored the movements of kinesin-coated Q-dots and dynein-coated Q-dots separately and together, that is, dual assay (see Supporting Information section 3 for details). The Q-dot trajectories for 20 s are plotted in Figure 3a for Q655-K, Figure 3b for Q655-D, and Figure 3c for both Q655-K and Q525-D, which indicates that the directions of Q-dots transported depend on the coated-motors. The results imply that the polarities of the microtubules oriented in the nanotracks reflect the moving direction of the motors for cargo transport.

In addition to moving directions, run length (RL) and velocity are key factors for mass transport of cargos because introducing both kinesin and dynein into the molecular system may deteriorate the motility of each of the motors. For kinesin, RL and velocity were 4.2 μm and 0.30 $\pm$ 0.10 μm s^{-1} (mean $\pm$ SE, N = 99), respectively, in the single assay (Q655-K) and 4.5 μm and 0.28 $\pm$ 0.10 μm s^{-1} (mean $\pm$ SE, N = 98) in the dual assay (Q655-K and Q525-D); for dynein, the respective values were 5.5 μm and 0.22 $\pm$ 0.10 μm s^{-1} (mean $\pm$ SE, N = 98) in the single assay (Q655-D), and 3.7 μm and 0.23 $\pm$ 0.15 μm s^{-1} (mean $\pm$ SE, N = 96) in the dual assay (Q655-K and Q525-D) (Supporting Information, Figures S4, S7, S8). These results, along with statistical analysis involving t tests showing nonsignificances among these results ($p > 0.1$; Student's t test), demonstrated that kinesin- and dynein-coated Q-dots retained their motility in the dual assay. In addition, RLs measured here using multiple motors were larger than those obtained with a smaller number of motors,[39,40] which increases the chance of Q-dot collisions resulting in efficient colocalization of them in the following experiments. The microtubule array, which is the first demonstration of parallel and individual microtubules with predefined polarities on nanotracks and supports motility of kinesin and dynein, is realized by integrating optimized approaches for microtubule gliding, etching of nanotracks, and microtubule dissociation.

Colocalization of Q-dots Carried by Kinesin and Dynein. Q-dot colocalization assay on the microtubule array was performed as follows after optimizing protein concentrations: Streptavidin-conjugated Q-dot 525 and Q-dot 655 were used in all experiments to evaluate colocalization mediated by the binding of either GST to GSH or streptavidin to biotin. We prepared GSH-Q525-D by conjugating the Q-dot 525 (10 nM) to biotin-PEG-GSH (25 nM), and then adding 100 nM dynein solution. For GST-Q655-K, we first incubated the Q-dot 655 (10 nM) in the presence of biotin-GFP-GST (25 nM), which was expressed in *Escherichia coli*. Kinesin was added at a final concentration of 100 nM. The colocalization assay was conducted on the microtubule array by sequentially injecting GSH-Q525-D, GST-Q655-K (each at a final concentration of 1 nM), and a 1 mM solution of ATP into a flow cell along with washing steps in between. Each washing step removes excess or unbound molecules from the flow cell. The subsequent molecular system is depicted in Figure 1b. Two Q-dots moved in opposite directions according to the polarity of the microtubule, and eventually some of the oppositely traveling Q-dots on the microtubule passed each other or became bound to each other.

In the experiment involving colocalization of bio-Q655-K and avi-Q525-D (Figure 1c), both streptavidin-labeled Q-dots were first coated only with motors (*i.e.*, Q655-K and Q525-D) to avoid two biotin moieties in a biotin–PEG–biotin molecule from attaching to the same Q-dot, thereby preventing adhesion. We first bound Q655-K (5 nM) to the microtubule array and then added biotin–PEG–biotin (0.5 μM) to produce bio-Q655-K. After eliminating the excess molecules by rinsing with solution BRB80, Q525-D (2 nM) in the ATP solution was introduced to the flow cell to start the colocalization assay. Using both GST–GSH and streptavidin–biotin molecular systems: GSH-Q525-D, GST-Q655-K, bio-Q655-K, and avi-Q525-D, we conducted the same experiments on microtubules randomly immobilized on a coverslip to evaluate RL, velocity, and colocalization (random microtubules in Figure 4d,e(iii)). This confirmed that the role of the nanotracks was restricted to orienting microtubule polarities to create the microtubule array, and that they did not affect the assay.

When designing the molecular structures, we also evaluated specific binding between GSH-Q525 and GST-Q655, and bio-Q655 and avi-Q525 without motors in bulk solution (bulk solution in Figure 4d,e(i)) and on a glass surface (glass surface in Figure 4d,e(ii)). Two Q-dots were simply mixed and incubated in bulk solution and then placed on a coverslip to visualize colocalizations. On a glass surface, molecules were sequentially

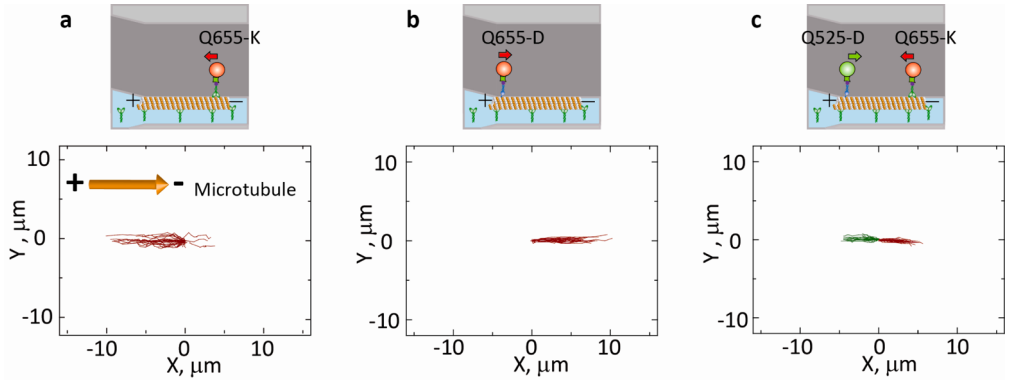

Figure 3. Conceptual diagrams and trajectories of Q-dots carried by kinesin or dynein on the microtubule array: (a) Q655-K ($N = 47$), (b) Q655-D ($N = 34$), and (c) Q655-K and Q525-D in a dual assay ($N = 53$) on the microtubule array. "*X*" and "*Y*" are the distance traveled parallel and perpendicular to the array, respectively.

immobilized, and finally the number of colocalized Q-dots was counted under a microscope. These molecular structures are illustrated as legend in Figure 4d,e, and experimental details are provided in the Supporting Information sections 4 and 5. In all control experiments for four experimental conditions, we omitted biotin–PEG–GSH or biotin–PEG–biotin molecules from the molecular systems described above.

As we examined the effects of mixing two motors in the dual assay, it is also necessary to evaluate how cargo molecules (GST, GSH, streptavidin, and biotin) affect motor activity. At optimal concentrations of Q-dots and proteins, the binding of cargo molecules to motors did not compromise motor functions. We measured both RL and velocity and compared the results with those obtained without conjugation to GST or GSH. The same measurement was also done using the streptavidin–biotin binding system. Comparison of the RLs and velocities of those labeled Q-dots confirmed that the binding of cargo molecules did not perturb the mobility of kinesin or dynein (Supporting Information, Figures S5–S8). In applications of motor proteins for molecular transport, roadblocks on microtubules are reported to hamper motility of motors.[41−44] Although such a phenomenon is critical in a gliding assay-based system[41,42] or single molecule level in a bead assay-based system,[43,44] long-distance transport by multiple motors in a bead assay-based system is stably achieved in our colocalization assay.

Massive and parallel Q-dot colocalizations on the microtubule array were realized using GST–GSH and streptavidin–biotin bindings. Overview of Q-dot transport according to the polarity of a microtubule array is captured in Figure 4a or Movie 2. Individual Q-dot motion could be analyzed if two Q-dots colocalized (Figure 4b, Movie 3) or passed one another (Figure 4c, Supporting Information, Movie 4). Since we recognized the bindings by spatial colocalizations of two fluorescent spots (red and green), there are possibilities to include false-positive detection caused by a nonspecific binding of two Q-dots or halting of motors. Therefore, we implemented the control experiments as described to evaluate significances of colocalizations due to GST–GSH or streptavidin–biotin bindings over molecular sequences without these binding molecules. In addition, some Q-dots might be colocalized before settling down and binding to a microtubule, we claimed Q-dot colocalizations when at least one of two Q-dots were motile on a microtubule and resulted in an overlapped Q-dot spot. Binding specificities in the control experiment ($N > 5$) were plotted in Figure 4d,e following normalization with the results obtained using the full molecular system (*i.e.*, lower values mean more specific binding, depending on the nature of the binding molecules). The value decreases with an increase in the number of specific binding events in the full molecular system. The full molecular systems are depicted in the legend for easier understanding.

For a GST–GSH molecular system (Figure 4d), binding specificities in (i) bulk solution and (ii) glass surface are 0.33 and 0.40, respectively. This means only 33% or 40% of Q-dots were colocalized when the GSH molecule was omitted in the control experiments. In other words, those colocalizations were caused nonspecifically. Specificities on (iii) random microtubules and (iv) the microtubule array are also calculated as 0.17 and 0.095, respectively. Kinesin motility on microtubules increased specificity of GST–GSH bindings. Streptavidin–biotin molecular system also showed higher specificities on random microtubules and the microtubule array as seen in GST–GSH system except the result in bulk solution (Figure 4e). This can be explained by the fact that the colocalization with the full molecular system decreased when both biotins of the biotin–PEG–biotin molecule bound to the same Q-dot in the bulk solution. The resulting specificity value was 0.61, which is the highest in all molecular systems investigated. Due to high specificity between streptavidin and biotin molecules, smaller values than the GST–GSH system are obtained: 0.055, 0.00, and 0.16 on (ii) a glass surface, (iii) randomly immobilized microtubules, and (iv) the microtubule array, respectively.

The increase of specificities on microtubules indicates that the designed GST–GSH or streptavidin–biotin

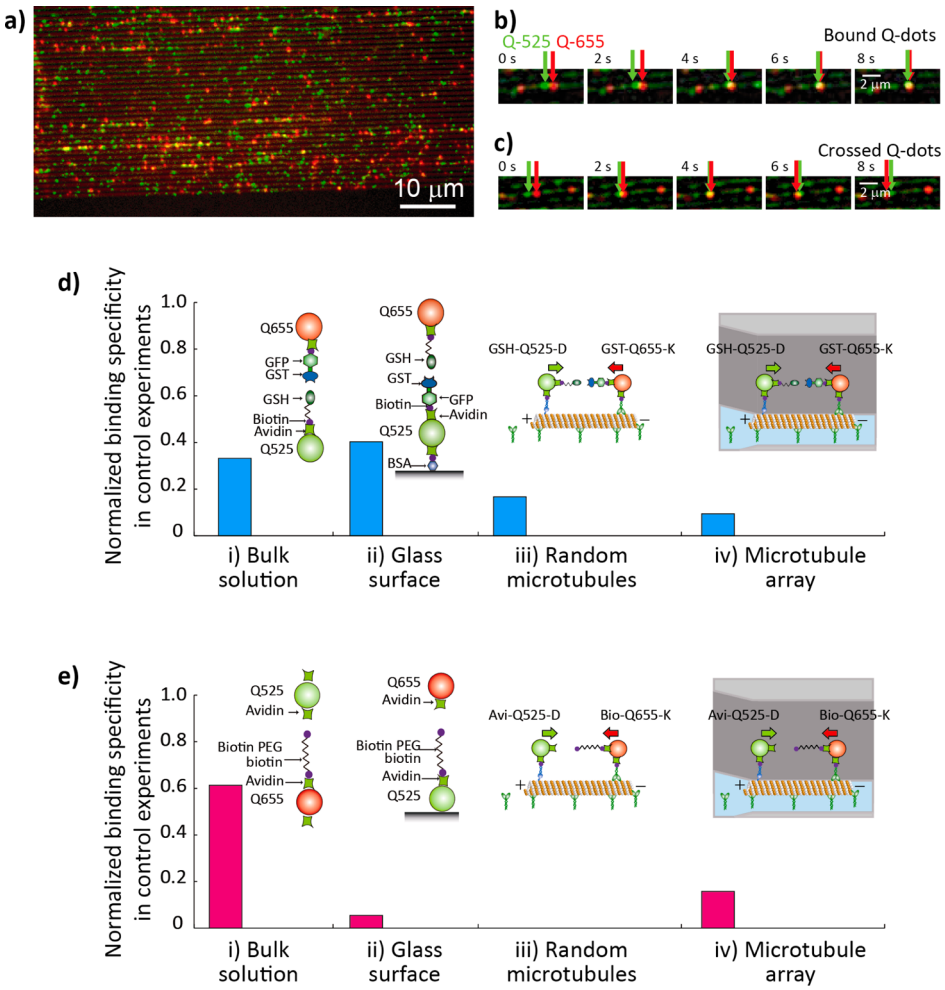

Figure 4. Q-dot binding assay on a microtubule array. (a) Q-dots on the microtubule array; (b) approaching and binding of two Q-dots; (c) approaching and crossing of two Q-dots; (d) binding specificity of the GST−GSH molecular system; (e) binding specificity of the streptavidin−biotin molecular system with schematic illustrations for each molecular binding.

molecules carried by motors induced more molecular specific bindings than those caused by diffusion in bulk solution or on a glass surface. Here, it should be noted that over 100 of colocalized Q-dots were counted for the results in bulk solution and on a glass surface, however, colocalizations on microtubules were ~10 Q-dots in a field of view (81.9 μm × 41.0 μm) and others passed one another even on the same microtubule. One of the reasons is the difference of Q-dot concentrations at binding of two Q-dots in four experimental conditions: 25 nM in bulk solution and ~1 nM on a glass surface or microtubules. Although Q-dot concentration was lowered for identifying individual Q-dots on a glass surface or microtubules, more colocalizations could be observed if we could increase the concentration. Another possible reason is that we could not control the position of motors on a microtubule at the collision of two Q-dots. Microtubules are composed of about 13 protofilaments depending on the polymerization condition. When two Q-dots, which are about to collide, might be carried by motors on different protofilaments of a microtubule, passing one another may be a result. In addition, since our microtubules were polymerized in BRB80, over 50% of them were expected to be composed of 14 protofilaments resulting in a counterclockwise helicity.[45] Motors moving on a protofilament follow this helicity and may interact with the nanotrack surface, which might decrease the number of colocalizations. To ensure the evaluation of specific bindings by GST−GSH or streptavidin−biotin, about 2-fold of Q-dots (>200 in a field of view) compared to full molecular systems were counted in the control experiments. Therefore, results prove that molecular binding was carried out in a massive and parallel manner under directional control of molecular transport *in vitro* at a Q-dot concentration of 1 nM. Compared with the concentrations in previously reported methods for GST or streptavidin[46,47] detection, our Q-dot concentration of 1 nM implies that GST−GSH or streptavidin−biotin bindings achieved in the system are applicable for detection in future.

CONCLUSION

In summary, we developed a novel method to orient individual microtubules to produce the microtubule

array with predefined polarities, which was achieved not only by a protein assay but also by integration of the nanofabrication of nanotracks and the microtubule dissociation method. The designed molecules using GST−GSH or streptavidin−biotin bindings demonstrated molecular specific bindings as a result of carrying cargo molecules by kinesin or dynein motors. Compared with *in vitro* applications based on a microtubule gliding assay, our MTAS will allow exploitation of motors involved in *in vivo* molecular transport for use with bead assay-based systems. MTAS, for which more functionality has yet to be demonstrated, is the first molecular platform that implements controlled and individual transport of target molecules to the designated direction for chemical reactions. The next challenge is how to utilize a specific protofilament of microtubule for further effective reactions. It will make MTAS close to practical applications to perform parallel and massive molecular reactions for a high-throughput screening.

MATERIALS AND METHODS

Nanotrack Fabrication. Borosilicate coverslips (26 mm ×34 mm, Matsunami Glass, Tokyo, Japan) were immersed in a 10 N KOH solution for at least 8 h and then washed thoroughly with deionized water. An aluminum layer was thermally deposited to a thickness of 150 nm. After a dehydration bake at 200 °C for 5 min, an electron beam resist (ZEP520A, Zeon Corp., Tokyo, Japan, diluted by addition of an equal volume of toluene) was spincoated at 4000 rpm for 90 s and baked at 180 °C for 2 min. Nanotracks were drawn by an electron beam writer with the optimal settings of 60 μC cm^{-2} and 400 pA. The resist layer was developed in ZED-B solution (Zeon Corp.) for 2 min and rinsed in ZMD-B (Zeon Corp.) for 10 min. The remaining aluminum layer was etched using an aluminum etchant (H_3PO_4:CH_3COOH:HNO_3 = 50:5:1) and washed with deionized water. The etching time was optimized to 8 min to create an overhang structure to ensure that microtubules were confined to nanotracks (Figure 2a).

Protein preparations. Tubulin was purified from porcine brains by two assembly disassembly cycles and phosphocellulose chromatography,[48] and stored in liquid nitrogen at 6 mg mL^{-1}. Tetramethyl rhodamine-conjugated tubulin was prepared by adding 10-fold molar excess of the dye to tubulin, resulting in a labeling stoichiometry of 1.3.[49] Unlabeled and labeled tubulin were mixed (10:1) and polymerized into microtubules for 30 min at 37 °C. A kinesin construct for microtubule gliding consisted of human kinesin (amino acid residues 1−573) with an N-terminal histidine tag. Another kinesin construct consisting of human kinesin (residues 1−465), an N-terminal histidine tag, and a C-terminal avi-tag was prepared to assay Q-dot transport. Both kinesins were purified as described.[26] Biotinylated dynein (SNAP647-labeled GST380) was a gift from Dr. Takahide Kon, Osaka University, Japan.[50] Tubulin was purified from porcine brain and stored at a concentration of 6 mg mL^{-1}. Fluorescently labeled tubulin was prepared by conjugation to tetramethyl rhodamine (C1711, Molecular Probes). Labeled and nonlabeled tubulins were mixed at the ratio of 1:10 and polymerized to labeled microtubules.

Microtubule Array in Nanotracks. Flow cells were constructed by placing two pieces of parafilm (25 × 5 mm^2) as spacers on a nanotrack-patterned coverslip, 5 mm apart, and covering them with a glass coverslip (18 × 18 mm^2, Matsunami Glass). Nanotracks were coated for 5 min with Pluronic F108 (3 mg mL^{-1}, F108, BASF), which transforms a hydrophobic ZEP520A surface to a hydrophilic surface that repels kinesin.[21] After clearing unbound material by washing with BRB80 buffer (80 mM PIPES, 1 mM EGTA, 1 mM $MgCl_2$, pH 6.8), 0.1 mg mL^{-1} kinesin (in BRB80 with 0.2 mg mL^{-1} casein) and 0.1 mg mL^{-1} paclitaxel-stabilized microtubules in BRB80 were introduced sequentially to the flow cell, with a 5-min incubation period and a 5-min washing step involving BRB80 for each. Densities of F/R-microtubules were measured by evaluating their gliding direction. The buffer was then replaced by an optimized oxygen scavenging system (36 μg mL^{-1} catalase, 1% β-mercaptoethanol, 20 mM dithiothreitol in BRB80) for microtubule dissociation (see Supporting Information section 2 for details). After exposure to light within the optimal wavelength range 530−550 nm for 5 s in area B (Figure 1a-2), microtubules in area A started gliding into nanotracks upon injection of an ATP solution (1 mM ATP in BRB-O_2, which comprised 36 μg mL^{-1} catalase, 25 mM glucose, 216 μg mL^{-1} glucose oxidase, 1% β-mercaptoethanol, and 20 mM dithiothreitol in BRB80 Figure 1a-3). Once the optimal assay time of 10 min had elapsed, microtubules were chemically immobilized by exposure to 0.1 wt % glutaraldehyde for 3 min, and then 0.1 M glycine for 5 min (Figure 2b). As discussed in the main text, over 90% of microtubules had the same polarity and guided Q-dot transport as a microtubule array (Figure 1a-4, Figure 3).

Optical Imaging and Image Processing. Microtubules and Q-dots were visualized using a fluorescent microscope (IX71, Olympus) equipped with a 100× oil objective (NA 1.3), a Dual-View image splitter (Optical Insights, LLC), and an electron multiplying charge-coupled device camera (iXon EM+ DU-897, Andor Technology PLC). Q525 and Q655 were spatially separated by the Dual-View splitter in the optical path and projected to the charge-coupled device. Acquired images and movies were processed using Andor iQ software.

Conflict of Interest: The authors declare no competing financial interests.

Supporting Information Available: Experimental methods and additional figures (Figures S1−S8), table of parameters (Table S1−S2) and movies. This material is available free of charge *via* the Internet at http://pubs.acs.org.

Acknowledgment. This work was supported by JST PRESTO program to R.Y. Electron beam lithography was conducted through the Kyoto-Advanced Nanotechnology Network, supported by the "Nanotechnology Network" of the Ministry of Education, Culture, Sports, Science and Technology (MEXT), Japan. The authors thank Ms. S. P. Subramaniyan with the Department of Micro Engineering Kyoto University, Japan, for critical reading of this paper.

REFERENCES AND NOTES

1. Manz, A.; Graber, N.; Widmer, H. M. Miniaturized Total Chemical Analysis Systems: A Novel Concept for Chemical Sensing. *Sens. Actuators B1* **1990**, 244–248.
2. Ueda, M.; Kiba, Y.; Abe, H.; Arai, A.; Nakanishi, H.; Baba, Y. Fast Separation of Oligonucleotide and Triplet Repeat DNA on a Microfabricated Capillary Electrophoresis Device and Capillary Electrophoresis. *Electrophoresis* **2000**, *21*, 176–180.
3. Woolley, A. T.; Mathies, R. A. Ultra-High-Speed DNA Fragment Separations Using Microfabricated Capillary Array Electrophoresis Chips. *Proc. Natl. Acad. Sci. U.S.A.* **1994**, *91*, 11348–11352.
4. Krishnan, M.; Namasivayam, V.; Lin, R.; Pal, R.; Burns, M. A. Microfabricated Reaction and Separation Systems. *Curr. Opin. Biotechnol.* **2001**, *12*, 92–98.
5. Kopp, M. U.; Mello, A. J.; Manz, A. Chemical Amplification: Continuous-Flow PCR on a Chip. *Science* **1998**, *280*, 1046–1068.
6. Zhang, C.; Xu, J.; Ma, W.; Zheng, W. PCR Microfluidic Devices for DNA Amplification. *Biotechnol. Adv.* **2006**, *24*, 243–284.
7. Mouradian, S. Lab-on-a-Chip: Applications In Proteomics. *Curr. Opin. Chem. Biol.* **2002**, *6*, 51–56.

8. Kuschel, M.; Neumann, T.; Barthmaier, P.; Kratzmeier, M. Use of Lab-on-a-Chip Technology for Protein Sizing and Quantitation. *J. Biomol. Tech.* **2002**, *13*, 172–178.
9. Stoughton, R. B. Applications of DNA Microarrays in Biology. *Annu. Rev. Biochem.* **2005**, *74*, 53–82.
10. Hibara, A.; Tsukahara, T.; Kitamori, T. Integrated Fluidic Systems on a Nanometer Scale and The Study on Behavior of Liquids in Small Confinement. *J. Chromatogr., A* **2009**, *1216*, 673–683.
11. Soto, C. M.; Martin, B. D.; Sapsford, K. E.; Blum, A. S.; Ratna, B. R. Toward Single Molecule Detection of Staphylococcal Enterotoxin B: Mobile Sandwich Immunoassay on Gliding Microtubules. *Anal. Chem.* **2008**, *80*, 5433–5440.
12. Rios, L.; Bachand, G. D. Multiplex Transport and Detection of Cytokines Using Kinesin-Driven Molecular Shuttles. *Lab Chip* **2009**, *9*, 1005–1010.
13. Hess, H.; Vogel, V. Molecular Shuttles Based on Motor Proteins: Active Transport in Synthetic Environments. *Rev. Mol. Biotechnol.* **2001**, *82*, 67–85.
14. Brunner, C.; Wahnes, C.; Vogel, V. Cargo Pick-up from Engineered Loading Stations by Kinesin Driven Molecular Shuttles. *Lab Chip* **2007**, *7*, 1263–1271.
15. Hiyama, S.; Gojo, R.; Shima, T.; Takeuchi, S.; Sutoh, K. Biomolecular-Motor-Based Nano- or Microscale Particle Translocations on DNA Microarrays. *Nano Lett.* **2009**, *9*, 2407–2413.
16. Taira, S.; Du, Y.-Z.; Hiratsuka, Y.; Konishi, K.; Kubo, T.; Uyeda, T. Q. P.; Yumoto, N.; Kodaka, M. Selective Detection and Transport of Fully Matched DNA by DNA-Loaded Microtubule and Kinesin Motor Protein. *Biotechnol. Bioeng.* **2006**, *95*, 533–538.
17. Byun, K.-E.; Choi, D. S.; Kim, E.; Seo, D. H.; Yang, H.; Seo, S.; Hong, S. Graphene—Polymer Hybrid Nanostructure-Based Bioenergy Storage Device for Real-Time Control of Biological Motor Activity. *ACS Nano* **2011**, *5*, 8656–8664.
18. Hiratsuka, Y.; Tada, T.; Oiwa, K.; Kanayama, T.; Uyeda, T. Q. Controlling the Direction of Kinesin-Driven Microtubule Movements Along Microlithographic Tracks. *Biophys. J.* **2001**, *81*, 1555–1561.
19. Yokokawa, R.; Takeuchi, S.; Kon, T.; Nishiura, M.; Sutoh, K.; Fujita, H. Unidirectional Transport of Kinesin-Coated Beads on Microtubules Oriented in a Microfluidic Device. *Nano Lett.* **2004**, *4*, 2265–2270.
20. Hutchins, B. M.; Platt, M.; Hancock, W. O.; Williams, M. E. Directing Transport of $CoFe_2O_4$-Functionalized Microtubules with Magnetic Fields. *Small* **2007**, *3*, 126–131.
21. Kim, T.; Kao, M. T.; Hasselbrink, E. F.; Meyhofer, E. Nanomechanical Model of Microtubule Translocation in the Presence of Electric Fields. *Biophys. J.* **2008**, *94*, 3880–3892.
22. Fischer, T.; Agarwal, A.; Hess, H. A Smart Dust Biosensor Powered by Kinesin Motors. *Nat. Nanotechnol.* **2009**, *4*, 162–166.
23. Hirokawa, N. Kinesin and Dynein Superfamily Proteins and the Mechanism of Organelle Transport. *Science* **1998**, *279*, 519–526.
24. Alberts, B.; Johnson, A.; Lewis, J.; Raff, M.; Roberts, K.; Walter, P., *Molecular Biology of the Cell, 4th ed.* 4th ed.; New York, 2002; p 1616.
25. Block, S. M.; Goldstein, L. S.; Schnapp, B. J. Bead Movement by Single Kinesin Molecules Studied with Optical Tweezers. *Nature* **1990**, *348*, 348–352.
26. Yokokawa, R.; Tarhan, M. C.; Kon, T.; Fujita, H. Simultaneous and Bidirectional Transport of Kinesin-Coated Microspheres and Dynein-Coated Microspheres on Polarity-Oriented Microtubules. *Biotechnol. Bioeng.* **2008**, *101*, 1–8.
27. Bohm, K.; Stracke, R.; Muhlig, P.; Unger, E. Motor Protein-Driven Unidirectional Transport of Micrometer-Sized Cargoes Across Isopolar Microtubule Arrays. *Nanotechnology* **2001**, *12*, 238–244.
28. Carroll-Portillo, A.; Bachand, M.; Greene, A. C.; Bachand, G. D. *In Vitro* Capture, Transport, and Detection of Protein Analytes Using Kinesin-Based Nanoharvesters. *Small* **2009**, *5*, 1835–1840.
29. Nitzsche, B.; Bormuth, V.; Bräuer, C.; Howard, J.; Ionov, L.; Kerssemakers, J.; Korten, T.; Leduc, C.; Ruhnow, F.; Diez, S., Chapter 14—Studying Kinesin Motors by Optical 3D-Nanometry in Gliding Motility Assays. In *Methods in Cell Biology*; Leslie, W., John, J. C., Eds.; Academic Press: 2010; Vol. 95, pp 247−271.
30. Lin, C. T.; Kao, M. T.; Kurabayashi, K.; Meyhofer, E. Self-Contained, Biomolecular Motor-Driven Protein Sorting and Concentrating in an Ultrasensitive Microfluidic Chip. *Nano Lett.* **2008**, *8*, 1041–1046.
31. Cheng, L. J.; Kao, M. T.; Meyhofer, E.; Guo, L. J. Highly Efficient Guiding of Microtubule Transport with Imprinted CYTOP Nanotracks. *Small* **2005**, *1*, 409–414.
32. Katira, P.; Agarwal, A.; Fischer, T.; Chen, H. Y.; Jiang, X.; Lahann, J.; Hess, H. Quantifying the Performance of Protein-Resisting Surfaces at Ultra-low Protein Coverages Using Kinesin Motor Proteins as Probes. *Adv. Mater.* **2007**, *19*, 3171–3176.
33. Hess, H.; Matzke, C. M.; Doot, R. K.; Clemmens, J.; Bachand, G. D.; Bunker, B. C.; Vogel, V. Molecular Shuttles Operating Undercover: A New Photolithographic Approach for the Fabrication of Structured Surfaces Supporting Directed Motility. *Nano Lett.* **2003**, *3*, 1651–1655.
34. Clemmens, J.; Hess, H.; Doot, R.; Matzke, C. M.; Bachand, G. D.; Vogel, V. Motor-Protein "Roundabouts": Microtubules Moving on Kinesin-Coated Tracks through Engineered Networks. *Lab Chip* **2004**, *4*, 83–86.
35. Lin, C.-T.; Kao, M.-T.; Kurabayashi, K.; Meyhofer, E. Efficient Designs for Powering Microscale Devices with Nanoscale Biomolecular Motors. *Small* **2006**, *2*, 281–287.
36. Jia, L.; Moorjani, S. G.; Jackson, T. N.; Hancock, W. O. Microscale Transport and Sorting by Kinesin Molecular Motors. *Biomed. Microdevices* **2004**, *6*, 67–74.
37. Nitta, T.; Tanahashi, A.; Obara, Y.; Hirano, M.; Razumova, M.; Regnier, M.; Hess, H. Comparing Guiding Track Requirements for Myosin- and Kinesin-Powered Molecular Shuttles. *Nano Lett.* **2008**, *8*, 2305–2309.
38. Harada, Y.; Sakurada, K.; Aoki, T.; Thomas, D. D.; Yanagida, T. Mechanochemical Coupling in Actomyosin Energy Transduction Studied by *in Vitro* Movement Assay. *J. Mol. Biol.* **1990**, *216*, 49–68.
39. Muthukrishnan, G.; Hutchins, B. M.; Williams, M. E.; Hancock, W. O. Transport of Semiconductor Nanocrystals by Kinesin Molecular Motors. *Small* **2006**, *2*, 626–630.
40. Thorn, K. S.; Ubersax, J. A.; Vale, R. D. Engineering the Processive Run Length of the Kinesin Motor. *J. Cell Biol.* **2000**, *151*, 1093–1100.
41. Schmidt, C.; Kim, B.; Grabner, H.; Ries, J.; Kulomaa, M.; Vogel, V. Tuning the "Roadblock" Effect in Kinesin-Based Transport. *Nano Lett.* **2012**, *12*, 3466–3471.
42. Korten, T.; Diez, S. Setting up Roadblocks for Kinesin-1: Mechanism for the Selective Speed Control of Cargo Carrying Microtubules. *Lab Chip* **2008**, *8*, 1441–1447.
43. Vershinin, M.; Carter, B. C.; Razafsky, D. S.; King, S. J.; Gross, S. P. Multiple-Motor Based Transport and its Regulation by Tau. *Proc. Natl. Acad. Sci. U.S.A.* **2007**, *104*, 87–92.
44. Dixit, R.; Ross, J. L.; Goldman, Y. E.; Holzbaur, E. L. Differential Regulation of Dynein and Kinesin Motor Proteins by Tau. *Science* **2008**, *319*, 1086–1089.
45. Ray, S.; Meyhöfer, E.; Milligan, R. A.; Howard, J. Kinesin Follows the Microtubule's Protofilament Axis. *J. Cell Biol.* **1993**, *121*, 1083–1093.
46. Chen, C. T.; Chen, W. J.; Liu, C. Z.; Chang, L. Y.; Chen, Y. C. Glutathione-Bound Gold Nanoclusters for Selective-Binding and Detection of Glutathione S-Transferase-Fusion Proteins from Cell Lysates. *Chem. Commun.* **2009**, 7515–7517.
47. Marinakos, S. M.; Chen, S. H.; Chilkoti, A. Plasmonic Detection of a Model Analyte in Serum by a Gold Nanorod Sensor. *Anal. Chem.* **2007**, *79*, 5278–5283.
48. Williams, R. C., Jr.; Lee, J. C. Preparation of Tubulin from Brain. *Methods Enzymol.* **1982**, *85 Pt B*, 376–385.
49. Hyman, A.; Drechsel, D.; Kellogg, D.; Salser, S.; Sawin, K.; Steffen, P.; Wordeman, L.; Mitchison, T. Preparation of Modified Tubulins. *Methods Enzymol.* **1991**, *196*, 478–485.
50. Numata, N.; Shima, T.; Ohkura, R.; Kon, T.; Sutoh, K. C-Sequence of the Dictyostelium Cytoplasmic Dynein Participates in Processivity Modulation. *FEBS Lett.* **2011**, *585*, 1185–1190.